A practical least-squares Kirchhoff Q migration workflow and its application to Celtic Sea imaging

Cheng Cheng, Yang He, Zhaojun Liu, Bin Wang (TGS)*

Summary

Least-squares migration in the data domain can improve the migration image illumination and mitigate the migration artifacts. But it requires many iterations of migration and demigration to obtain the desired subsurface reflectivity model, which can limit its wide use in production. As for Kirchhoff migration, the main purpose of the least-squares method is to remove the migration artifacts and random noise, improve image illumination and amplitude fidelity under complex velocity, which can be fully addressed by image domain least-squares migration. Adding the Q effect into the least-squares migration process can compensate for amplitude loss due to attenuation in the gas zone and can correct the image phase. We investigate the application of image-domain least-squares Kirchhoff migration and least-squares Kirchhoff Q migration with adaptive curvelet-domain matching filters, used as an inverse Hessian operator. A practical workflow together with a 3D field data example in an offshore Ireland Atlantic dataset demonstrates reduced image artifacts, improved amplitude behavior and stable Q compensation.

Introduction

Since the traditional ray-based migration approaches are computationally efficient in imaging and model building, this kind of migration is widely applied for industrial production. However, the seismic application to under-sampled and irregularly acquired seismic data causes migration noise and swing artifacts, as well as uneven illumination of the image. An appropriate preprocessing sequence can help mitigate these problems, but the underlying issue remains. Least-squares (LS) migrations (Schuster, 1993; Nemeth et al., 1999) have been introduced into the industry for decades. Their application estimates the image of the reflectivity model where the modeled data best fit the observed data in the least-squares sense. LS migration can fundamentally account for uneven acquisition geometry, complex overburdens, and migration artifacts. It can be classified as LS Kirchhoff migration (Nemeth et al., 1999), LS one-way wave-equation migration (Lu et al., 2017) and LS reverse-time migration (Dai et al., 2013; Zhang et al., 2015). Here we use the LS Kirchhoff migration approach to obtain a shallow image with better image quality and improved illumination. We also include attenuation in the least-squares migration scheme to give the overall effect of an attenuation-compensating prestack depth migration. We demonstrate the improvement in both image quality and Q compensation with a North Sea data set. Different from LS wave-equation migration, the LS Kirchhoff would not change the spectrum of the migration image, since the demigrated data set should have the same spectrum content as the original input data set.

Methodology

1. True amplitude antialiasing Kirchhoff demigration: The demigration can be regarded as the Born forward modeling with the reflectivity model (usually regarded as the migration image) in a smooth background velocity model. The efficiency and accuracy of migration and demigration operators are crucial for applying the least-squares migration algorithm. Our Kirchhoff demigration approach is implemented in the common-shot or common-CDP domain with a repeated use of traveltime tables. The raw demigrated data shows many aliased signals. This operator aliasing occurs when the input data spacing is too coarse and the frequency is too high for the steep migration operator summation trajectory. A reduced CDP interval in migration image can mitigate this problem, but with additional computation and GPU memory cost. For better data quality, we implement the antialiasing with the triangle filter following Lumley et al. (1994), which was first developed for migration. We extend this method to Kirchhoff demigration so we can do antialiasing on the fly to further accelerate the computation. Our new operator anti-aliasing method preserves the optimal resolution that the input data provides, while suppressing the aliased energy without any dip constraint and additional computation.

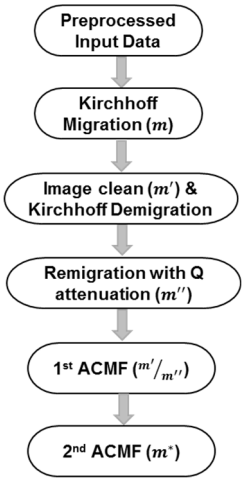

Figure 1: Workflow chart for ACMF LS Kirchhoff Q migration.

10.1190/segam2019-3214151.1

To provide useful information for AVO analysis, it is meaningful to have a true-amplitude Kirchhoff demigration, which is implemented here following Zhang et al. (2002). This gives us a true amplitude compliant demigration operator. Then similar to He et al. (2018), we demigrate on cleaned stacked image with constant AVO. Any AVO variation observed after remigration is considered to arise from the model or the acquisition geometry, which can be corrected by later adaptive matching filters.

2. LS Kirchhoff migration with curvelet-domain adaptive matching filter:

LS migration inverts for the true reflectivity model m to fit the field data d. The image-domain least-squares solution to this inverse problem is:

$$m^* = (L^T L)^{-1} L^T d, \quad (1)$$

where L^T is migration operator, L is the adjoint of migration operator denoted as a demigration operator and $(L^T L)^{-1}$ is the inverse Hessian opeartor. Since direct calculation of this inverse opeartor is not practical, many approaches have been proposed to approximate it, including the point spread functions (Lecomte, 2008), pseudodifferential operators (Guo et al, 2017), or curvelet-domain Hessian filters (Wang et al., 2016). To match events with different dips, an adaptive curvelet matching filter (ACMF), which is implemented through solving an optimization problem (Zhai et al., 2017), is adopted here. As the flow shows in Figure 1, first, a matching filter is derived from two reference image gathers. We first construct a reference image gather m' by cleaning the original image m. Then demigration is done for all offsets on m' to generate synthetic data $d' = Lm'$. A remigration is followed to generate the synthetic migration:

$$m'' = L^T d' = L^T L m', \quad (2)$$

So, by matching the remigrated image gather m'' to the cleaned image gather m', we can estimate the adaptive matching filter $(L^T L)^{-1}$ for each offset. It consists of the inverse of a combination operator, the forward modeling and migration operators, which fundamentally are determined by the model, the underlying migration method and the acquisition geometry. Then this $(L^T L)^{-1}$ is applied to the original migration results m to generate the inversion result m^* at the final stage.

3. Q compensation as a byproduct of least-squares:

Although conventional Q compensating migration methods are highly accurate in handling complex Q models in theory, they can be susceptible to noise and artifact boosting. As a contrast, adding seismic-wave attenuation into the image-domain, one iteration of a least-squares workflow generates a stable boost of weak signal without sacrificing the quality of the overall image. Our approach of implementing the Q compensation during the least-squares process is similar to the method Casasanta et al. (2017) describe. Rather than a more computation-consuming viscoacoustic Kirchhoff demigration, we only use one attenuating remigration

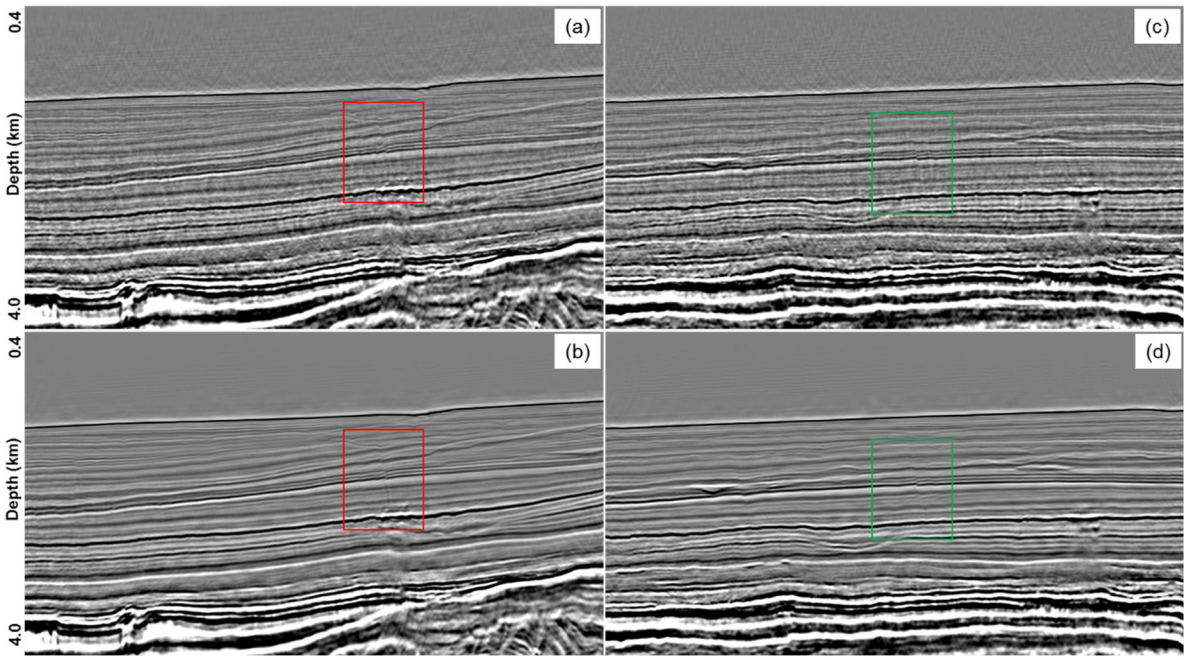

Figure 2: (a) Raw Kirchhoff common offset migraiton image in Inline direction and (c) Xline direction. (b) LS Kirchhoff common offset migration image in Inline direction and (d) Xline direction.

10.1190/segam2019-3214151.1

operator and normal migration/demigration operator. Now equation (2) becomes:

$$m'' = L_Q^T d' = L_Q^T L m', \quad (3)$$

where L_Q^T denotes a migration operator with the same amplitude and phase behavior of the viscoacoustic modeling operator. Rather than applying a Q compensation, the operator continues attenuating amplitude and distorting phase. By matching m'' to the cleaned image gather m', the adaptive matching filter $(L_Q^T L)^{-1}$ estimate not only accounts for migration swing but also compensates for amplitude and phase due to Q absorption for each offset. This is applied later to m to generate m^* free of artifacts and Q compensated. The complete workflow for this image domain least-squares Q Kirchhoff migration is shown in Figure 1.

CREAN data example

We demonstrate our proposed workflow with a 2017 3D Crean narrow-azimuth survey off the western coast of Ireland, in the Porcupine Basin area of the Celtic Sea, covering about 5500 km^2. This is a triple-source acquisition configuration. The new acquisition was merged with approximately 960 km^2 of legacy data, and the entirety was reprocessed together. Higher resolution seismic can be acquired without reducing the cable spacing by increasing the number of sources from two to three. The shot interval is reduced to maintain CMP fold, resulting in an overlap between shot records. The receiver and cable spacing are 37.5 m, after the necessary preprocessing including survey matching, deblending, multiple attenuation. The offsets in this study range from ~100 m to ~8000 m. The final data are then input to our LS Kirchhoff Q migration workflow. The high-resolution anisotropic velocity and Q models were derived from a sequence of image-guided tomographic inversion and multistage FWI (Hilburn and Mao, 2019).

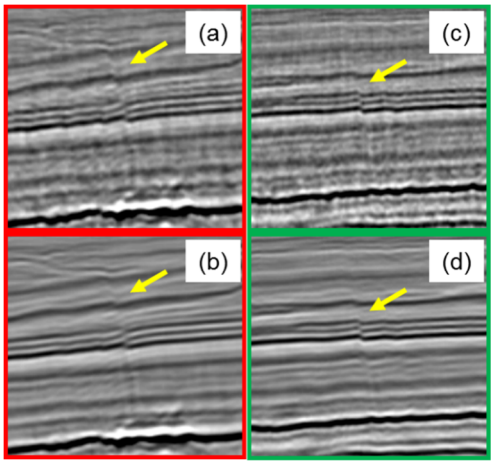

Figure 3: Zoom in of the windows in Figure 2. (a) Raw Kirchhoff migraiton image in Inline direction. (b) LS Kirchhoff migration image in Inline direction. (c) Raw Kirchhoff migraiton image in Xline direction. (d) LS Kirchhoff migration image in Xline direction.

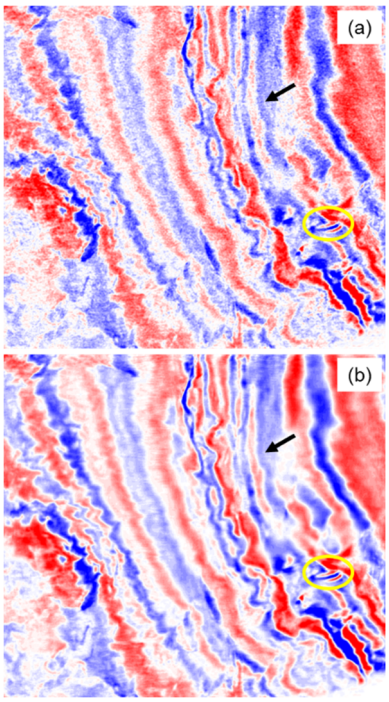

Figure 4: Depth view of (a) raw Kirchhoff migration (b) LS Kirchhoff migration.

The initial Kirchhoff migration image shows poor migration swing cancellation in the inline direction (Figure 2a), especially in the shallow part, using a standard antialiasing parameter, which is also observed in the crossline direction (Figure 2c). A dense trace interpolation can reduce the noise but with a lower resolution in the shallow image, especially where dipping fault structure in the shallow are smeared. Also, this will add additional cost to migration and demigration. We apply our least-squares Kirchhoff migration to fully remove the migration artifact without sacrificing the quality and frequency content of the original migration image. The S/N in the image domain LS Kirchhoff migration common-offset image is much higher than in the raw migration image, after the migration swing is highly reduced, in both inline and crossline direction (Figure 2b, d). The expanded image Figure 3 of the window in Figure 2 shows that faults and complex shallow features (yellow arrow in Figure 3) are well preserved and clearer after the overlapping swing is reduced. Figure 4 shows the depth view comparison between LS migration and migration. The channel events indicated by the black arrow shows more continuity and fidelity. Small and complex features indicated by a yellow circle is well preserved, which indicates no loss

10.1190/segam2019-3214151.1

of horizontal wavenumber. For different field data cases, the parameter for least-squares weight in the curvelet matching can be tuned to select better retention of the fault structure or more attenuation of the swing noise. This will need careful QC in the image domain case-by-case.

Just like LS RTM, our LS Kirchhoff migration improves amplitude fidelity, because it further corrects for non-uniform illumination by the round-trip (demigration plus remigration) approximation of Hessian. Figure 5 shows the comparison between the raw migration gathers and LS migration gathers. Cleaner gathers and more uniform AVO for further interpretation are achieved.

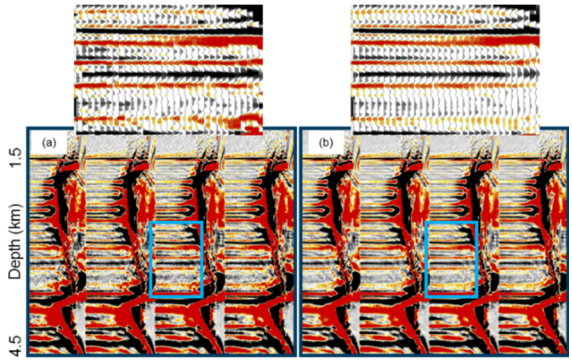

Figure 5: (a) Raw Kirchhoff migration gathers. (b) LS Kirchhoff migration gathers. The variable wiggle review corresponds to the zoomed in portion on the gathers.

Some shallow anomalies in our 3D image volume, expected to be related to gas features, distort the image in their vicinity and in deeper sediments. This can be observed as significant sags in underlying image features and the loss of high frequencies inside and immediately below the anomalies. Initial imaging in this area reveals a neatly structured shallow sedimentary region, which persists down from 2 km to a thick chalk layer at 3.5 km in depth (Figure 6). As can be seen in Figure 6a, this shallow region is contaminated by anomalies characterized by significant sags in underlying layers. This is due to severely blurring events in the migrated gathers, suggesting very sharp velocity contrasts. The imaging impact of the largest of these anomalies can be observed more than two kilometers below its upper bounds. As a demonstration of an efficient image domain least-squares Q migration, we apply our workflow to this data where obvious Q absorption is observed.

Comparing the standard migration with the least-squares migration, neither containing Q, (Figures 6a and 6c) we see a degree of reduced noise and swing artifacts. Figures 6a and 6b compare a standard migration with a Q-compensating migration, showing the uplift in resolution obtained by including Q compensation in the standard migration. However, as can be seen clearly from these two images, the unwanted migration artifacts are also boosted up which severely contaminate the image. The least-squares Q migration image in Figure 6d contains the best of both worlds: improved event coherency, more balanced illumination, reduced noise and swings, and a stable increase in resolution. The adaptive curvelet filter derived from our image matching method can account for noise removal, amplitude balancing and phase correction.

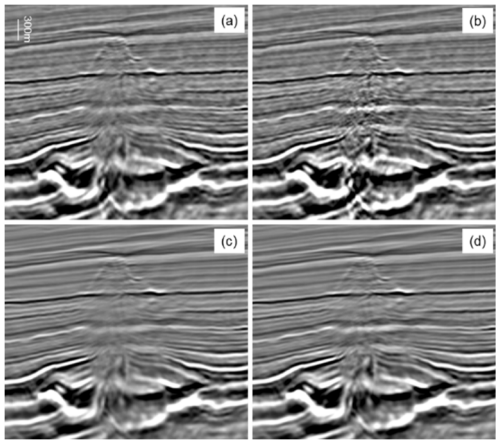

Figure 6: (a) Raw Kirchhoff migration. (b) Kirchhoff Q migration. (c) LS Kirchhoff migration. (d) LS Kirchhoff Q migration.

Conclusion

We have built an efficient image-domain least-squares Kirchhoff Q migration flow and applied it to a triple source 3D survey. Improved imaging of the complex and potentially prospective structures in the area is achieved. The result shows that compared to conventional Kirchhoff migration, our LS Kirchhoff migration can mitigate the migration swing artifacts caused by sparse fold coverage and imperfect acquisition geometry, without losing any resolution of faults or complex structure. The final imaging result also shows that by efficiently including attenuation in this least-squares migration process, a stable improvement in image resolution and amplitude fidelity is obtained below the depth affected by Q absorption. Deeper sediments of exploration at gas pockets and channels which initially contaminated the underlying image are better resolved.

Acknowledgements

We would like to thank the management of TGS-NOPEC for permission to publish these study results and images. We thank Alex Yeh and Chris Chiang for software assistance. A special thanks to Connie VanSchuyver for help reviewing this paper.

10.1190/segam2019-3214151.1

REFERENCES

Casasanta, L., F., Perrone, G., Roberts, A., Ratcliffe, and K., Purcell, 2017, Applications of single-iteration Kirchhoff least-squares migration: 87th Annual International Meeting, SEG, Expanded Abstracts, 4432–4435, doi: https://doi.org/10.1190/segam2017-17704075.1.

Dai, W., Y., Huang, and G. T., Schuster, 2013, Least-squares reverse time migration of marine data with frequency-selection encoding: Geophysics, **78**, no. 4, S233–S242, doi: https://doi.org/10.1190/geo2013-0003.1.

Guo, P., H., Guan, R., Nammour, B., Duquet, and G. A., McMechan, 2017, A stable Q compensation approach for adjoint seismic imaging by pseudodifferential scaling: 87th Annual International Meeting, SEG, Expanded Abstract, 4566–4571, doi: https://doi.org/10.1190/segam2017-17747338.1.

He, Y., F., Hao, S., Dong, and B., Wang, 2018, Towards AVO compliant least-squares RTM gathers: 88th Annual International Meeting, SEG, Expanded Abstracts, 4408–4412, doi: https://doi.org/10.1190/segam2018-2997421.1.

Hilburn, G., and J., Mao, 2019, High-resolution multistage FWI and image-guided tomography to resolve ultraslow gas anomalies: 81st Annual International Conference and Exhibition, EAGE, Extended Abstracts, Accepted, doi: https://doi.org/10.3997/2214-4609.201901569.

Lecomte, I., 2008, Resolution and illumination analyses in PSDM: A ray-based approach: The Leading Edge, **27**, 650–663, doi: https://doi.org/10.1190/1.2919584.

Lu, S., X., Li, A. A., Valenciano, N., Chemingui, and C., Cheng, 2017, Broadband least-squares wave-equation migration: 87th Annual International Meeting, SEG, Expanded Abstracts, 4422–4425, doi: https://doi.org/10.1190/segam2017-17634859.1.

Lumley, D. E., J. F., Claerbout, and D., Bevc, 1994, Anti-aliased Kirchhoff 3-D migration: 64th Annual International Meeting, SEG, Expanded Abstracts, 1282–1285, doi: https://doi.org/10.1190/1.1822760.

Nemeth, T., C., Wu, and G. T., Schuster, 1999, Least-squares migration of incomplete reflection data: Geophysics, **64**, 208–221, doi: https://doi.org/10.1190/1.1444517.

Schuster, G. T., 1993, Least-squares cross-well migration: 63rd Annual International Meeting, SEG, Expanded Abstracts, 110–113, doi: https://doi.org/10.1190/1.1822308.

Wang, P., A., Gomes, Z., Zhang, and M., Wang, 2016, Least-squares RTM: Reality and possibilities for subsalt imaging: 86th Annual International Meeting, SEG, Expanded Abstracts, 4204–4209, doi: https://doi.org/10.1190/segam2016-https://doi.org/13867926.1.

Zhai, Y., Z., Liu, J., Sheng, B., Wang, and J., Heim, 2017, A hybrid crossgather curvelet domain multiple elimination method and its application: 87th Annual International Meeting, SEG, Expanded Abstract, 4752–4757, doi: https://doi.org/10.1190/segam2017-17741149.1.

Zhang, Y., L., Duan, and Y., Xie, 2015, A stable and practical implementation of least-squares reverse time migration: Geophysics, **80**, no. 1, V23–V31, doi: https://doi.org/10.1190/geo2013-0461.1.

Zhang, Y., M., Karazincir, C., Notfors, J., Sun, and B., Hung, 2002, Amplitude preserving v(z) pre-stack Kirchhoff migration, demigration and modeling: 64th Annual International Conference and Exhibition, EAGE, Extended Abstracts, B-11.